DOR: 20.1001.1.27170314.2023.12.3.5.2

Research Paper

Optimization of Fused Deposition Modeling Process Parameters to Achieve Maximum Mechanical Properties Using Response Surface Methodology

Ali Hasanabadi[1*], Hossein Afshari[1], Seyyed Mohammad Bagher Mirafzali[1]
[1]Mechanical Engineering Department, University of Birjand, Birjand, Iran
[*]Email of the Corresponding Author: hasanabadi@birjand.ac.ir
Received: August 1, 2023; Accepted: November 17, 2023

Abstract
In this study, the researchers investigated the impact of various parameters, including layer raster angle, infill extrusion width, and layer height, on mechanical properties such as tensile strength, elongation, and Young's modulus of polylactic acid printed samples. To reduce experimental costs, the Box-Behnken method was employed along with response surface methodology using Minitab software to establish the relationship between input and output variables. The results of the tension test indicated that the raster angle had a significant impact on all three properties. Furthermore, the regression equations showed that changes in infill extrusion width and layer height had a strong effect on tensile strength but had a less significant impact on elongation and Young's modulus. The optimal output parameters were determined to be 38.67 MPa tensile strength, 3.42% elongation, and 1117.47 MPa Young's modulus using input parameters of 10 degree raster angle, 170% infill extrusion width, and 0.2 mm layer height. The study validated the results obtained through experimental testing and concluded that the response surface methodology could predict part properties with high accuracy (less than 6% error) based on input parameters.

Keywords
Fused Deposition Modeling, Mechanical Properties, Polylactic Acid, Response Surface Methodology

Symbols and Abbreviations

SLA	stereolithography	SEM	scanning electron microscopy
FDM	fused deposition modeling	A	raster angle (degree)
PLA	polylactic acid	B	infill extrusion width (%)
ABS	acrylonitrile butadiene styrene	C	layer height (mm)
PC	polycarbonate	σ	tensile strength (MPa)
PA12	nylon 12 filament	d_i	Individual desirability function
ANOVA	analysis of variance	D	Total desirability function
SLS	selective laser sintering		

1. Introduction

Additive manufacturing methods are attracting the attention of researchers from different disciplines due to the ease of production, as well as the favorable physical and mechanical characteristics of

printed parts. There are various methods for 3D printing, but their main common feature is the addition of materials in a layer on top of the previous layer, unlike machining, which is performed by gradually removing the material to achieve the final form of the workpiece. In these methods, first, the model is designed with the help of computer-aided design software, and then, using additive manufacturing technology, materials are layered on top of each other to become a physical product [1-4].

There are several methods for manufacturing parts with the help of 3D printing, two of the most important of which are stereolithography (SLA) and the other one is fused deposition modeling (FDM) [5]. The FDM method is one of the most common methods of 3D printing parts, which was first invented in 1989 by Crump [6]. This method has many applications in various industries such as machinery, automobile manufacturing, medicine, and aerospace due to several advantages such as proper strength, flexibility, high production speed, biocompatibility, and biodegradability, as well as the possibility of manufacturing parts with complex geometry [7-10].

In the FDM method, the raw material in the form of a filament, which is mostly made of plastic, is heated in the nozzle of the printer by a heater. Then, the paste material comes out from the orifice of the nozzle in the form of thin strings and is arranged continuously, and it is placed on top of each other in the direction of the movement of the nozzle, creating a three-dimensional volume. In the hardware part of the device, a numerical control unit is used which is responsible for moving the nozzle [11-13].

Due to the wide range of FDM methods, much research has been done on this method. Hasanzadeh et al [14] investigated the effects of process input parameters on the impact strength of polylactic acid (PLA) parts produced by the FDM method. In this research, the infill percentage, layer lamination angle, and layer thickness changes were considered as input parameters. The results of their research showed that the infill percentage is the most effective parameter, and by reducing it, the impact strength also decreases.

Patterson et al. [15] investigated the limitations and problems of manufacturing parts by FDM method. In this research, three types of filament PLA, acrylonitrile butadiene styrene (ABS), and polycarbonate (PC) were used to make parts, and then the indicators that lead to limitations were identified. Nabipour et al [16] investigated the effects of printing parameters on the tensile strength of polymer-metal composite parts made by the FDM method. In this research, copper powder is used as a metal component with a weight percentage of 25%, and granules as a polymer component with a weight percentage of 75%. Nozzle diameter, layer thickness, filling pattern, and nozzle temperature are also selected as process input parameters. Bottini et al. [17] developed a new method to describe the roughness profile in the process of fusion deposition. Brajlih et al. [18] investigated the effects of print speed on the dimensional accuracy of stereolithography production parts. Zarko et al. [19] examined the production of embossed molds by 3D printer and FDM method. The results of their research showed that as the print speed increases, the dimensional accuracy of the models decreases and the worst print speed is equal to 90 mm/s. Rinanto et al. [20] also investigated the effect of input parameters for printing, including infill percentage, extrusion temperature, and layer lamination angle. They used Taguchi's experimental design and investigated the effects of input parameters on tensile strength, energy consumption, and processing time. Next, they optimized the input parameters of the process to achieve the highest amount of tensile strength and the lowest amount of energy consumption and processing time. The results of their research showed that the most optimal value

for the parameters is at the extrusion temperature of 210°C, the layer lamination angle of 45° and the infill percentage of 40%. Feng et al. [21] investigated the tensile strength of parts made with nylon 12 filament (PA12) and filament produced with recycled polyamide powder, using the selective laser sintering (SLS) method. They investigated the effect of printing speed and manufacturing direction and concluded that if the printing speed is too high or too low, the mechanical properties are strongly affected. By examining the tensile strength, flexural modulus, and impact strength of the manufactured parts, they concluded that the X direction has the best-mentioned properties. Farmarzian et al. [22] designed and built a porous structure of the Schwarz P type. It was made by the FDM method and the material used was PLA. An increase in the percentage of porosity leads to a decrease in strength and an increase in the size of cells in a constant porosity leads to an increase in Young's modulus. Shadvar et al. [23] investigated the extrusion of polycaprolactone using the FDM method. In this process, the effects of various parameters such as the volume rate of the material, the geometry of the extruder and nozzle, and the temperature of the melt formation area on the quality of the final piece have been examined.

Amouhadi et al. [24] investigated the effect of shell thickness parameters and manufacturing direction on the accuracy of external dimensions, as well as obtaining a prediction model and error compensation. The obtained results indicate that increasing the thickness of the shell causes a decrease in dimensional accuracy, and the 45-degree direction has the highest dimensional accuracy. Naghieh et al. [25] fabricated bone scaffolds by FDM method. They simulated the mechanical behavior of the produced scaffold with the finite element model and compared it with each other. Karnan et al. [26] investigated the bending and compressive strength of the workpiece made with PLA-Cu composite filament. They examined the effect of temperature and layer thickness on bending and impact strength. They concluded that higher nozzle temperature and substrate temperature improved compressive and bending strength. Patil et al [27] investigated multi-objective optimization of FDM parameters for parts made with PLA material. They concluded that it is essential to have a suitable set of input parameters such as layer thickness, infill percentage, infill pattern, temperature, printing speed, and other parameters. Giri et al [28] optimized 3D printing parameters in the FDM process by a neural network. They optimized the critical parameters of the process such as layer thickness, air gap, layer width, manufacturing direction, and filling angle. They concluded that fabrication orientation is the most important parameter for optimal results.

In the FDM method, several parameters affect the mechanical properties of the produced parts. Some of the most important effective parameters in this method include layer thickness, filling angle, manufacturing direction, filling density, printing speed, filling pattern, extrusion temperature, nozzle diameter, and air gap between layers [29]. Despite the much research that has been conducted in this field, the way process parameters affect the mechanical properties of parts is still a challenging issue, and many methods such as artificial neural networks, genetic algorithms, fuzzy analysis, and response surface methodology are used for parameters optimization [30]. In the current research, among the many parameters, the effect of factors such as raster angle, infill extrusion width, and layer height on the mechanical properties of the parts prepared by the FDM method is investigated using the response surface methodology. Due to the high number of input parameters, there is a need for a large number of experiments. To reduce the number of tests appropriately, the Box-Behnken method is used.

2. Methodology

Response surface methodology is used as an optimization method in various research fields [31, 32]. In this research, using the design of the experiment with the help of response surface and Box-Behnken method using Minitab software, the effects of layer raster angle, infill extrusion width, and layer height on the results of the tensile test of the samples prepared from PLA is investigated in the FDM process. The use of synthetic polymers has increased due to their cheap price and favorable mechanical properties. Among the polymers that can be used, environmental polymers are of special interest, and polylactic acid can be mentioned in this context [33, 34], which is used in the current research.

The box-Behnken method is an incomplete three-level factorial design. In this method, a block of two-level experiments is repeated among different sets of variables. This scheme is presented to solve the problem of a large number of experiments (samples) in a design with a large number of factors. The number of tests in this method is kept constant in such a way that it is sufficient to estimate the coefficients of the quadratic equation. For each of the input parameters, three levels are considered. Table 1 shows the levels of these parameters.

The values of the parameter levels are determined based on previous research [35-37] and experimental verification.

It should be noted that the infill extrusion width parameter is related to the extruder part of the printer and is considered as a percentage of the extrusion width in normal mode. The higher the percentage, the more material is used and as a result, the layers will be thicker. Since the overall infill density is constant, as the layers get thicker, their distances will increase.

Table 1. Levels of experimental design parameters

Parameter	Symbol	Level 1	Level 2	Level 3
Raster angle (degree)	A	0	45	90
Infill extrusion width (%)	B	100	150	200
Layer height (mm)	C	0.1	0.2	0.3

Other parameters that are considered as fixed parameters for all samples are presented in Table 2.

Table 2. Fixed settings of printer parameters

Print speed (mm/s)	40
Nozzle diameter (mm)	0.3
Filament diameter (mm)	1.75
Extrusion temperature (°C)	210
Bed temperature (°C)	60

Using the considered parameter levels in Table 1, the experimental design Table 3 has been created using the Box-Behnken method, which includes 15 test samples.

To evaluate the tensile strength, elongation to break, and Young's modulus, all samples were designed and printed according to the ASTME8 standard for each test as shown in Figures 1 and 2 respectively. The test samples were printed by an Alpha30 model printer made by Keytec company. To perform the tensile test, the STM-250 tensile testing machine made by the SANTAM company was used. Tensile testing for all samples has been done at ambient temperature with a test speed of 10 mm/min.

Based on the obtained force-displacement curves, the values of tensile strength, elongation, and Young's modulus are given in Table 3.

Table 3. Experiments designed by Box-Behnken method and results of tensile test

Sample number	Raster angle (degree)	Infill extrusion width (%)	Layer height (mm)	Maximum load (kN)	Tensile strength (MPa)	Elongation(%)	Young's modulus (MPa)
1	0	100	0.2	1.27	32.06	3.21	971.72
2	45	200	0.3	1.32	33.80	3.19	1059.89
3	90	200	0.2	1.33	34.43	3.57	964.13
4	45	200	0.1	1.39	30.81	2.54	1166.85
5	0	150	0.3	1.5	38.36	3.75	1014.38
6	45	100	0.1	1.22	30.81	3.62	858.59
7	90	150	0.3	1.33	33.44	3.94	846.34
8	90	150	0.1	1.24	31.76	3.70	857.61
9	0	200	0.2	1.47	35.54	3.67	971.76
10	90	100	0.2	1.29	32.81	4.13	790.46
11	45	150	0.2	1.40	38.00	3.13	1183.76
12	0	150	0.1	1.37	35.22	3.59	971.72
13	45	150	0.2	1.41	38.22	3.13	1059.89
14	45	150	0.2	1.39	37.71	3.13	964.13
15	45	100	0.3	1.35	31.28	3.16	1166.85

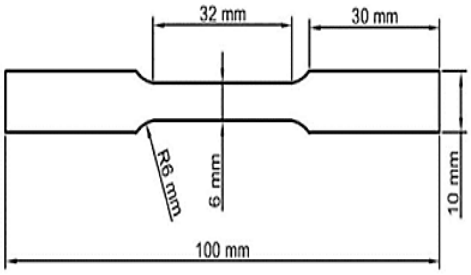

Figure 1. Tensile test specimen dimensions

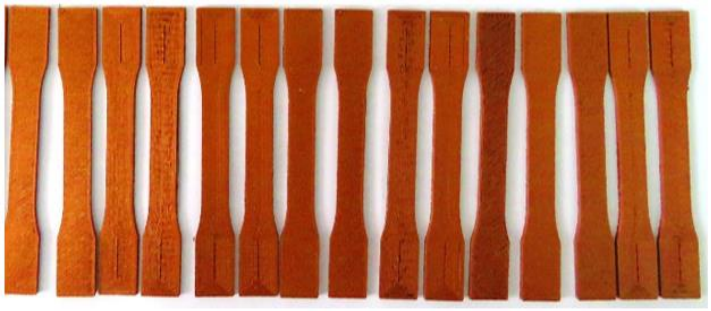

Figure 2. Printed samples according to the test design Table 2

3. Results and discussion

3.1 Analysis of variance

Table 3 shows the results of the tensile test of the printed samples according to the specified parameters. To find out how the input parameters relate to the tensile strength, elongation, and Young's modulus of the samples, an analysis of variance is used. The validity of the assumed model is checked by using quadruple diagrams of residual plots as depicted in Figure 3. Due to the absence of a specific pattern in the residual diagram and the bell-shaped histogram, the validity of the model is confirmed.

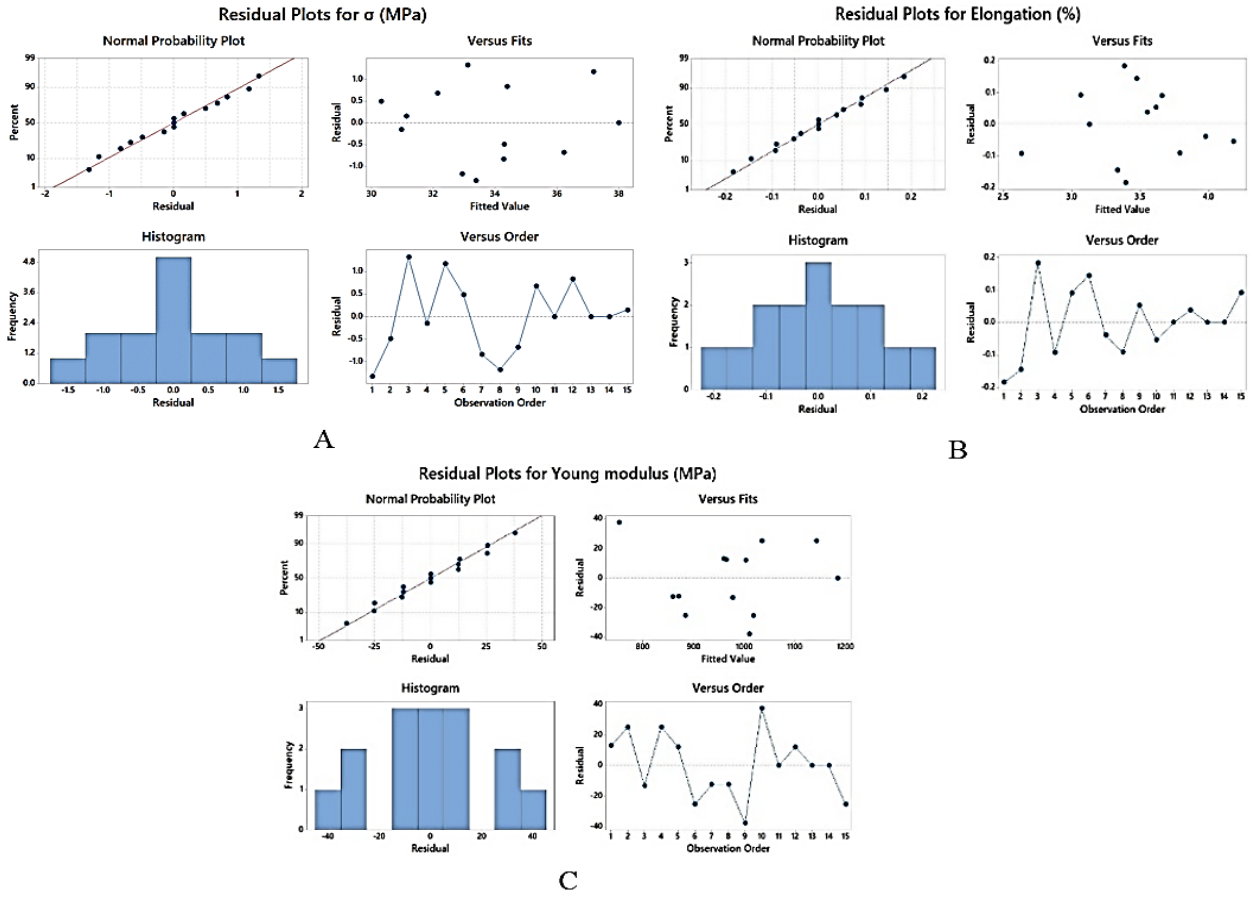

Figure 3. Residual plots for tensile strength (A), elongation (B), and Young's modulus (C)

Analysis of variance (ANOVA) tables are calculated as Tables 4, 5, and 6 for tensile strength, elongation, and Young's modulus respectively. It is assumed that if the p-value is less than 0.05, the corresponding item will be significant.

Table 4. Analysis of variance for tensile strength

Source	DF	Seq SS	Contribution	Adj SS	Adj MS	F-Value	P-Value
Model	9	99.009	91.58%	99.0085	11.0009	6.04	0.031
Linear	3	25.376	23.47%	25.3763	8.4588	4.65	0.066
A	1	9.548	8.83%	9.5485	9.5485	5.24	0.071
B	1	7.258	6.71%	7.2580	7.2580	3.99	0.102
C	1	8.570	7.93%	8.5698	8.5698	4.71	0.082
Square	3	70.647	65.35%	70.6468	23.5489	12.93	0.009
A*A	1	0.125	0.12%	1.4888	1.4888	0.82	0.407
B*B	1	44.199	40.88%	49.3256	49.3256	27.09	0.003
C*C	1	26.322	24.35%	26.3221	26.3221	14.46	0.013
2-Way Interaction	3	2.985	2.76%	2.9854	0.9951	0.55	0.672
A*B	1	0.865	0.80%	0.8649	0.8649	0.48	0.521
A*C	1	0.533	0.49%	0.5329	0.5329	0.29	0.612
B*C	1	1.588	1.47%	1.5876	1.5876	0.87	0.393
Error	5	9.103	8.42%	9.1033	1.8207	-	-
Lack-of-fit	3	6.050	5.31%	6.0502	1.6262	0.81	0.593
Pure Error	2	3.054	3.11%	3.0539	2.0152	-	-
Total	14	108.112	100.00%	-	-	-	-
$R^2 = 91.58$ %							

Table 5. Analysis of variance for elongation

Source	DF	Seq SS	Contribution	Adj SS	Adj MS	F-Value	P-Value
Model	9	2.15317	93.40%	2.15317	0.23924	7.86	0.018
Linear	3	0.36563	15.86%	0.36563	0.12188	4.01	0.085
A	1	0.15680	6.80%	0.15680	0.15680	5.15	0.072
B	1	0.16531	7.17%	0.16531	0.16531	5.43	0.067
C	1	0.04351	1.89%	0.04351	0.04351	1.43	0.285
Square	3	1.21782	52.83%	1.21782	0.40594	13.34	0.008
A*A	1	1.19781	51.96%	1.18390	1.18390	38.91	0.002
B*B	1	0.01124	0.49%	0.00970	0.00970	0.32	0.597
C*C	1	0.00878	0.38%	0.00878	0.00878	0.29	0.614
2-Way Interaction	3	0.56972	24.71%	0.56972	0.18991	6.24	0.038
A*B	1	0.26010	11.28%	0.26010	0.26010	8.55	0.033
A*C	1	0.00160	0.07%	0.00160	0.00160	0.05	0.828
B*C	1	0.30802	13.36%	0.30802	0.30802	10.12	0.024
Error	5	0.15213	6.60%	0.15213	0.03043	-	-
Lack-of-fit	3	0.05012	2.49%	0.05012	0.01414	0.30	0.817
Pure Error	2	0.10201	4.11%	0.10201	0.04672	-	-
Total	14	2.30529	100.00%	-	-	-	-

R^2 = 93.40 %

Table 6. Analysis of variance for Young's modulus

Source	DF	Seq SS	Contribution	Adj SS	Adj MS	F-Value	P-Value
Model	9	237862	97.41%	237862	26429	20.93	0.002
Linear	3	66435	27.21%	66435	22145	17.53	0.004
A	1	28332	11.60%	28332	28332	22.43	0.005
B	1	37751	15.46%	37751	37751	29.89	0.003
C	1	353	0.14%	353	353	0.28	0.620
Square	3	148811	60.94%	148811	49604	39.27	0.001
A*A	1	102505	41.98%	116252	116252	92.05	0.000
B*B	1	21146	8.66%	24708	24708	19.56	0.007
C*C	1	25160	10.30%	25160	25160	19.92	0.007
2-Way Interaction	3	22616	9.26%	22616	7539	5.97	0.042
A*B	1	7537	3.09%	7537	7537	5.97	0.058
A*C	1	598	0.24%	598	598	0.47	0.522
B*C	1	14482	5.93%	14482	14482	11.47	0.020
Error	5	6315	2.59%	6315	1263	-	-
Lack-of-fit	3	2152	0.74%	2152	654	0.35	0.817
Pure Error	2	4165	1.85%	4165	1872	-	-
Total	14	244176	100.00%	-	-	-	-

R^2 = 97.41 %

The regression equations that relate the values of tensile strength, elongation, and Young's modulus to the input parameters are expressed as Eqs. (1), (2) and (3) respectively.

$$\sigma(\text{MPa}) = -8.39 + 0.0512\ A + 0.4417\ B + 101.9\ C - 0.000314\ A^2 - 0.001462\ B^2 - 267.0\ C\times C - 0.000207 A\times B - 0.081\ A^*C + 0.126\ B\times C \quad (1)$$

$$\text{Elongation}(\%) = 4.51 - 0.00594\ A - 0.0027\ B - 9.74\ C + 0.000280\ A^2 - 0.000021\ B^2 + 4.88\ C^2 - 0.000113\ A\times B + 0.0044\ A\times C + 0.0555\ B\times C \quad (2)$$

$$\text{Young's modulus}(\text{MPa}) = -475 + 4.21\ A + 12.73\ B + 5296\ C - 0.08762\ A^2 - 0.03272\ B^2 - 8255\ C^2 + 0.01929\ A\times B - 2.72\ A\times C - 12.03\ B\times C \quad (3)$$

3.2 Effect of parameters on the mechanical properties

The mean effects of input parameters on tensile strength, elongation, and Young's modulus are shown in Figures 4, 5 and 6 respectively.

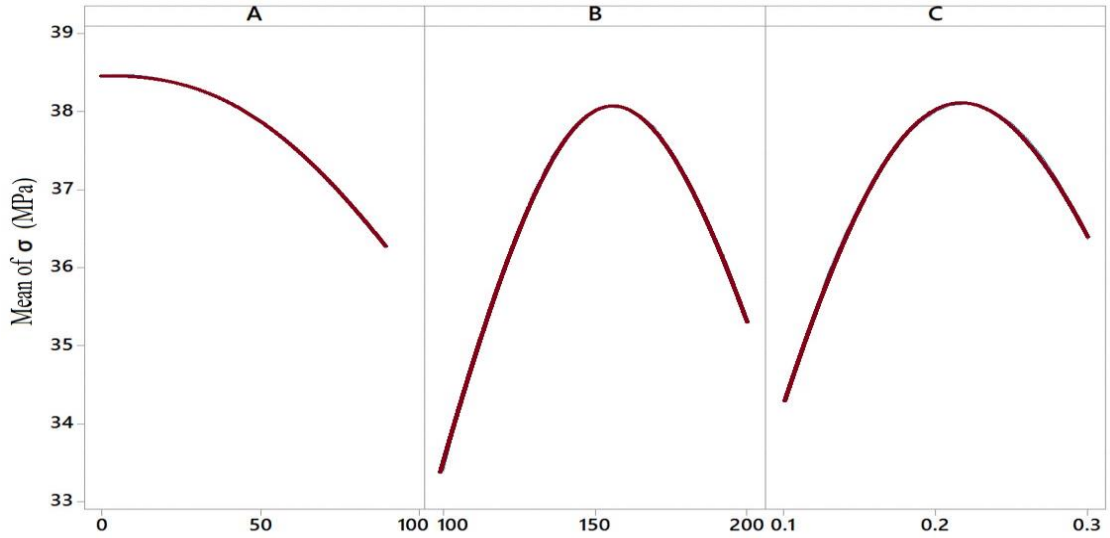

Figure 4. Effects of input parameters on tensile strength of printed samples

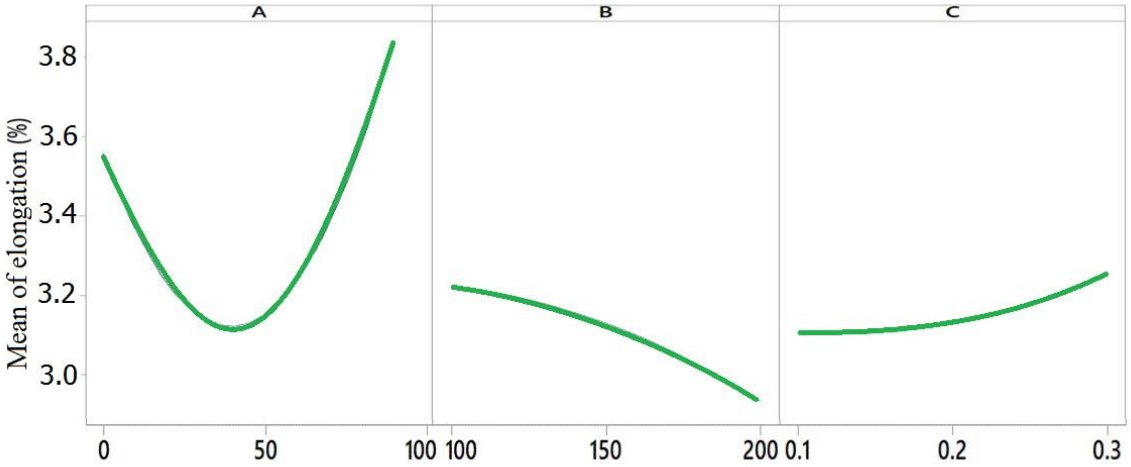

Figure 5. Effects of input parameters on the elongation of printed samples

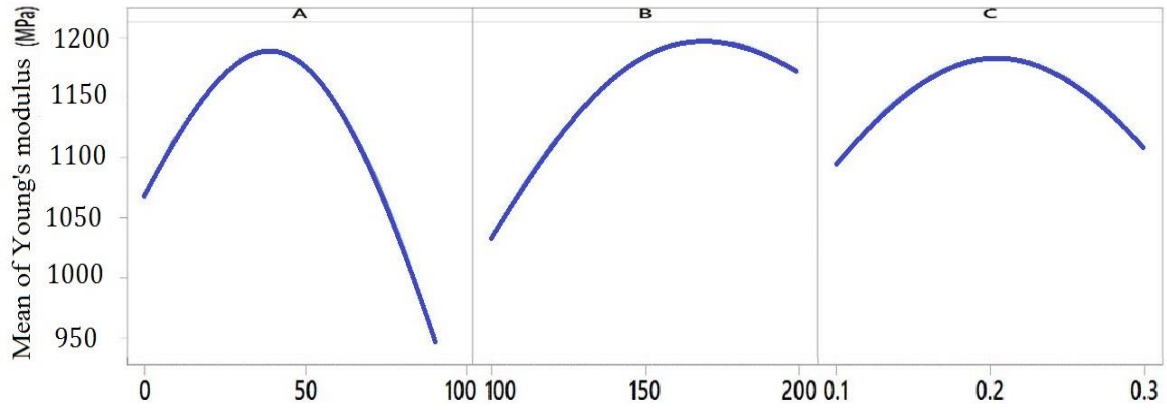

Figure 6. Effects of input parameters on the Young's modulus of printed samples

Figure 4 shows that increasing the raster angle always has a negative effect on the tensile strength. The best angle is the zero angle which provides the most strength. But increasing the infill extrusion width and the height of the layers first increases the strength, and after reaching a maximum value, decreases the strength. The highest obtained tensile strength is equal to 38.36 MPa for zero raster angle, 150 infill, and 0.3 layer height. On the other hand, the lowest value of strength is equal to 30.81 MPa, and its difference with the highest value is equal to 24.5%, and this shows the importance of paying attention to the correct setting of the parameters.

Figure 5 shows that increasing the raster angle first reduces the elongation but from about 45° onwards, increasing the raster angle increases the amount of elongation. It can also be seen that the changes in the other two parameters do not have much effect on elongation. The highest amount of elongation obtained for the sample with 90° raster angle, is equal to 4.13%.

Figure 6 shows that for all three parameters, the trend of changes in Young's modulus is similar. That is, with the increase of the input parameters, the Young's modulus increases, and after a certain value, the Young's modulus will decrease. The maximum value of Young's modulus in tests was equal to 1183.76 MPa for the sample with a raster angle equal to 45°.

Figure 7 demonstrates the scanning electron microscope (SEM) images of the fracture surface of sample number four (Table 3) with 0.1 layer height, 45 raster angle, and 200% infill extrusion width with different magnifications. The images are taken from the center of the cross-section. In Figure 7(a), the connections between the layers are clearly depicted. In Figure 7(e), it is evident that the lateral connection between the layers is not well-established, resulting in voids between them. Considering that sample number four has less elongation than all samples, the brittle fracture of the sample is clear in the images.

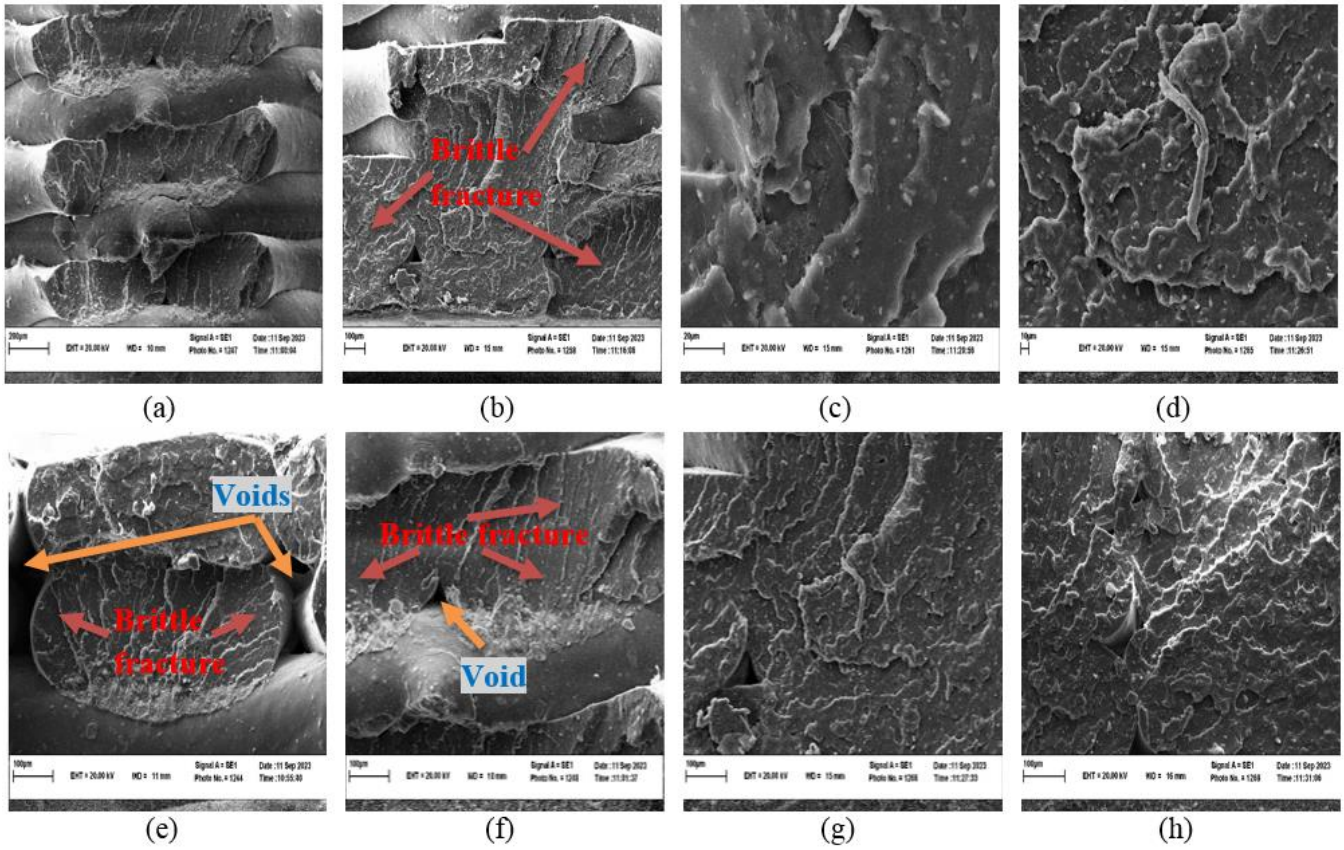

Figure 7. SEM images of the fracture surface of sample number four with different magnifications

3.3 Optimization of mechanical properties

Optimizing input parameters including raster angle, layer height, and infill extrusion width to achieve maximum values of tensile strength, elongation, and Young's modulus simultaneously can be done with the help of Minitab software optimizer. Using the desirability function for each property, d_i, (Equation 4) it is possible to calculate the total desirability function, D using Equation 5 [38-40].

$$d_i = \begin{cases} 0 & y_i < L \\ \dfrac{y_i - L}{T - L} & L \le y_i \le T \\ 1 & y_i > T \end{cases} \qquad (4)$$

where y_i is a desired property, T is the upper limit of that property and L is the lower one. D can be calculated as:

$$D = (d_1 d_2 \dots d_m)^{\frac{1}{m}} \qquad (5)$$

By maximization of Equation 5, for $m = 3$, optimum output properties are obtained at 38.67 MPa, 3.42%, and 1117.47 MPa for tensile strength, elongation, and Young's modulus, respectively whereas the optimal input parameters are 10 degrees, 170% and 0.2 mm for raster angle, infill extrusion width and layer height respectively as depicted in Figure 8.

To verify the obtained results, a new sample with optimal input parameters was printed and tested. Table 7 demonstrates the differences between the optimal sample properties provided by software

and the printed sample. The maximum error between the optimization and experiment results is less than 6%.

Table 7. Comparison of predicted properties based on regression equations and experiment for the optimal sample with 10° raster angle, 170 % infill extrusion width, and 0.2 mm layer height

Property	Minitab optimizer	Experiment	Error (%)
Tensile strength (MPa)	38.67	36.84	4.73
Elongation(%)	3.42	3.38	1.46
Young's modulus	1117.74	1053.81	5.69

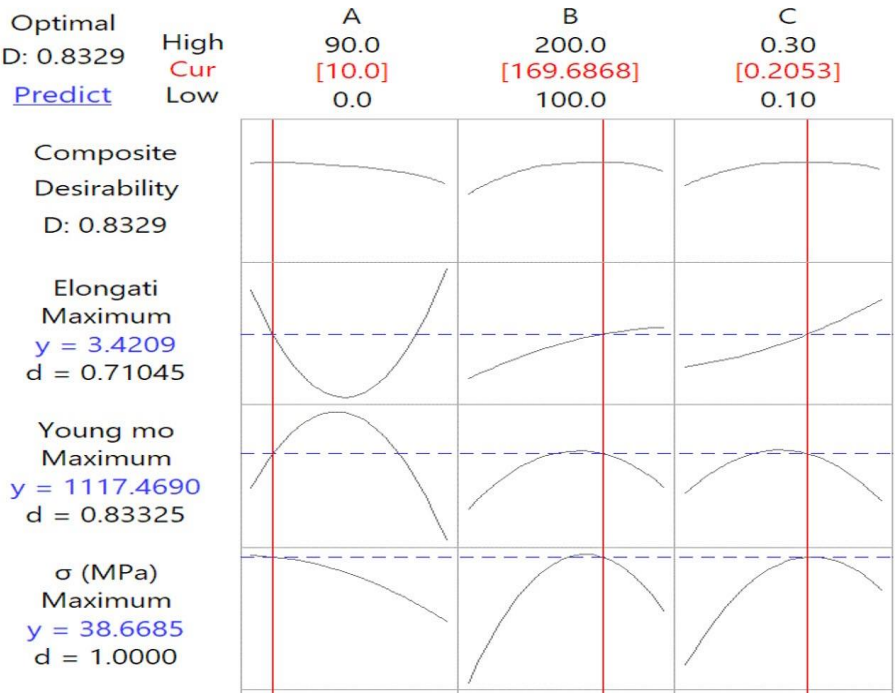

Figure 8. Graphs resulting from optimization using Minitab optimizer; optimum input parameters to yield maximum output properties are determined

4. Conclusions

Using the response surface accompanying the Box-Behnken method is a suitable method for studying the effects of input parameters on output properties at a lower cost with fewer tests. In this research, the relationship between raster angle, infill extrusion width, and height of layers with tensile strength, elongation, and Young's modulus was investigated using this method. Examining the resulting regression relationships showed that the raster angle has a great effect on tensile strength, elongation, and Young's modulus. Examining the effect of two other parameters, including infill extrusion width and layer height, showed that the tensile strength was highly affected by these two factors, while elongation and Young's modulus were less affected. Maximum values for tensile strength, elongation, and Young's modulus were 38.22 MPa, 4.13%, and 1183.76 MPa respectively. However, optimization of all properties simultaneously predicted optimal input parameters as 10° for raster angle, 170% for infill extrusion width and 0.2 mm for layer height and output parameters as 38.67 MPa for tensile strength, 3.42% for elongation and 1117.47 MPa for Young's modulus where the maximum difference with the experimental results was less than 6%.

5. References

[1] Shahrubudin, N., Lee, T.C., and Ramlan, R. 2019. An Overview on 3D Printing Technology: Technological Materials, and Applications. Procedia Manufacturing. 35:1286-1296. doi: 10.1016/j.promfg.2019.06.089.

[2]Arumaikkannu, G., Anilkumar, N., and Saravanan, R. 2008. Study on the influence of rapid prototyping parameters on product quality in 3D printing. International Solid Freeform Fabrication Symposium. Texas, USA.

[3]Chua, C.K., Leong, K.F. and Lim, C.S. 2010. Rapid prototyping: principles and applications. World Scientific Publishing Company. Singapore.

[4]Yao, T., Deng, Z., Zhang, K. and Li, S. 2019. A method to predict the ultimate tensile strength of 3D printing polylactic acid (PLA) materials with different printing orientations. Composites Part B: Engineering.163:393-402. doi:10.1016/j.compositesb.2019.01.025.

[5]Srivastava, M., Maheshwari, S., and Kundra, T. 2015. Virtual modelling and simulation of functionally graded material component using FDM technique. Materials Today: Proceedings. 2:3471-3480. doi: 10.1016/j.matpr.2015.07.323.

[6]Waran, V., Narayanan, V., Karuppiah, R. Owen, S. and Aziz, T. 2013. Utility of multimaterial 3D printers in creating models with pathological entities to enhance the training experience of neurosurgeons. Technical note. Journal of neurosurgery, 120(2):489-492. doi: 10.3171/2013.11.JNS131066.

[7]Vaezi, M., Chianrabutra, S., Mellor, B., and Yang, S. 2013. Multiple material additive manufacturing–Part 1: a review: Virtual and Physical Prototyping. 8:19-50. doi: 10.1080/17452759.2013.778175

[8]Han, S.H., Cha, M., Jin, Y.Z., Lee, K.M. and Lee, J.H. 2020. BMP-2 and hMSC dual delivery onto 3D printed PLA-Biogel scaffold for critical-size bone defect regeneration in rabbit tibia. Biomedical Materials. 16(1):015019. doi:10.1088/1748-605X/aba879.

[9]Moreno, R., Carou, D., Alvarez, D.C. and Gupta, M.K. 2020. Statistical models for the mechanical properties of 3D printed external medical aids. Rapid Prototyping Journal. 27(1):176-186. doi: 10.1108/RPJ-02-2020-0033.

[10] Pucci, J.U., Christophe, B.R., Sisti, J.A. and Connolly E.S. 2017. Three-dimensional printing: technologies, applications, and limitations in neurosurgery. Biotechnology advances. 35(5):521-529. doi:10.1016/j.biotechadv.2017.05.007.

[11] Zein, I., Hutmacher, D.W, Tan, K.C. and Teoh, S. H. 2002. Fused deposition modeling of novel scaffold architectures for tissue engineering applications. Biomaterials. 23(4):1169-1185. doi:S0142-9612(01)00232-0.

[12] Peng, A., Xiao, X. and Yue, R. 2014. Process parameter optimization for fused deposition modeling using response surface methodology combined with fuzzy inference system. The International Journal of Advanced Manufacturing Technology. 73:87-100. doi:10.1007/s00170-014-5796-5.

[13] Hongyao, S., Xiaoxiang, Y. and Jianzhong, F. 2018. Research on the flexible support platform for fused deposition modeling. The International Journal of Advanced Manufacturing Technology. 97:3205-3221. doi:10.1007/s00170-018-2046-2.

[14] Hasanzadeh, R. and Azdast, T. 2021. Optimization of FDM 3D Printing Process Parameters of Biodegradable Poly Lactic Acid Polymeric Samples (in Persian). Modares Mechanical Engineering. 21(2):69-78. dor:20.1001.1.10275940.1399.21.2.2.8.

[15] Patterson, A.E., Chadha, C. and Jasiuk, I.M. 2021. Identification and Mapping of Manufacturability Constraints for Extrusion-Based Additive Manufacturing. Journal of Manufacturing and Materials Processing. 5(2):33. doi:10.3390/jmmp5020033.

[16] Nabipour, M., Behravesh, A.H. and Akhoundi, B. 2017. Effect of printing parameters on Mechanical Strength of Polymer-Metal composites Printed via FDM 3D printer (in Persian). Modares Mechanical Engineering. 17(1):145-150. dor:20.1001.1.10275940.1396.17.1.38.8.

[17] Bottini, L. and Boschetto. 2014. Surface Characterization in Fused Deposition Modeling in Surface Engineering Techniques and Applications: Research Advancements. IGI Global publishing. doi:10.4018/978-1-4666-5141-8.ch008.

[18] Brajlih, T., Valentan, B., Balic, J. and Igor, D. 2011. Speed and accuracy evaluation of additive manufacturing machines. Rapid Prototyping Journal. 17(1):64-75. doi:10.1108/13552541111098644.

[19] Žarko, J.,Vladić, G., Pál, M. and Dedijer, S. 2017. Influence of printing speed on production of embossing tools using FDM 3D printing technology. Journal of Graphic Engineering and Design. 8(1):19-27. doi:10.24867/JGED-2017-1-019.

[20] Rinanto, A., Nugroho, A., Prasetyo, H.and Pujiyanto, E. 2018. Simultaneous Optimization of Tensile Strength, Energy Consumption and Processing Time on FDM Process Using Taguchi and PCR-TOPSIS. 4th International Conference on Science and Technology (ICST). Yogyakarta. Indonesia. doi:10.1109/ICSTC.2018.8528667.

[21] Feng, L. Wang, Y. and Wei, Q. 2019. PA12 powder recycled from SLS for FDM. Polymers. 11(4):727. doi:10.3390/polym11040727.

[22] Faramarzian Haghighi, A., Haerian Ardakani, A., Kafaee Razavi, M. and Moloodi, A. 2019. Simulation of Mechanical Behavior and Construction of Regular PLA Scaffolds (in Persian). Modares Mechanical Engineering. 19(8):1953-1958. dor: 20.1001.1.10275940.1398.19.8.9.7

[23] Shadvar, N., Badrossamay, M. and Foroozmehr, E. 2016. Modelling of polycaprolactone extrusion in additive manufacturing process by fused deposition modelling in ansys-polyflow software. Modares Mechanical Engineering. 15(13):440-444.

[24] Amouhadi, I., Foroozmehr, E. and Badrossamay, M. 2016. Experimental analysis of the effects of contour width and built orientation on dimensional accuracy of FDM made parts and introducing an error prediction model. Modares Mechanical Engineering. 15(13):445-449.

[25] Naghieh, S., Karamooz Ravari, M.R., Badrossamay, M., Foroozmehr, E. and Kadkhodaei, M. 2016. Finite element analysis for predicting the mechanical properties of bone scaffolds fabricated by fused deposition modeling (FDM). Modares Mechanical Engineering. 15(13):450-454.

[26] Karnan, B., Pavan, M., Ali, S.K. and Gnaniar, K. 2021. Compression and flexural study on PLA-Cu composite filament using FDM. Materials Today: Proceedings. 44(1):1687-1691. doi:10.1016/j.matpr.2020.11.858.

[27] Patil, P., Singh, D., Raykar, S. and Bhamu, J. 2021. Multi-objective optimization of process parameters of Fused Deposition Modeling (FDM) for printing Polylactic Acid (PLA) polymer components. Materials Today: Proceedings. 45(6):4880-4885. doi:10.1016/j.matpr.2021.01.353.

[28] Giri, J., Shahane, P., Jachak, S., Chadge, R. and Giri, P. 2021. Optimization of FDM process parameters for dual extruder 3D printer using Artificial Neural network. Materials Today: Proceedings. 43(5):3242-3249. doi:10.1016/j.matpr.2021.01.899.

[29] Dey, A. andYodo, N. 2019. A Systematic Survey of FDM Process Parameter Optimization and Their Influence on Part Characteristics. Journal of Manufacturing and Materials Processing. 3(3):64. doi:10.3390/jmmp3030064.

[30] Suniya, N.K., Verma, A.K. 2023. A review on optimization of process parameters of fused deposition modeling. Research on Engineering Structures & Materials. 9(2):631-659. doi:10.17515/resm2022.520ma0909

[31] Choopani, Y. and Razfar, M.R. 2014. Investigation of the Effective Parameters on Surface Roughness in Magnetic Abrasive Finishing Process Using Design of Experiments. Journal of Modern Processes in Manufacturing and Production. 3(1):17-25.

[32] Lotfi, M., Amini, S., Sajjady, S.A. and Juaifer, A.H. 2018. The Effectiveness of Ceramic Wiper Tool in Turning of Monel K500. Journal of Modern Processes in Manufacturing and Production. 7(2):47-64.

[33] Casasola, R., Thomas, N.L., Trybala, A. and Georgiadou, S. 2014. Electrospun poly lactic acid (PLA) fibres: Effect of different solvent systems on fibre morphology and diameter. Polymer. 55(18):4728-4737 doi:10.1016/j.polymer.2014.06.032.

[34] Balakrishnan, H., Hassan, A., Imran, M. and Wahit, M.U. 2012. Toughening of Polylactic Acid Nanocomposites: A Short Review. Polymer-Plastics Technology and Engineering. 51(2):175-192. doi:10.1080/03602559.2011.618329.

[35] Liu, X., Zhang, M., Li, S., Si, L., Peng, J. and Hu, Y. 2017. Mechanical property parametric appraisal of fused deposition modeling parts based on the gray Taguchi method. The International Journal of Advanced Manufacturing Technology. 89:2387-2397. doi:10.1007/s00170-016-9263-3.

[36] Samykano, M. 2021. Mechanical property and prediction model for FDM-3D printed polylactic acid (PLA). Arabian Journal for Science and Engineering. 46:7875-7892. doi:10.1007/s13369-021-05617-4.

[37] Yao, T., Ye, J., Deng, Z., Zhang, K. Ma, Y. and Ouyang, H. 2020. Tensile failure strength and separation angle of FDM 3D printing PLA material: Experimental and theoretical analyses. Composites Part B: Engineering. 188:107894. doi:10.1016/j.compositesb.2020.107894.

[38] Isapour Rudy, M., Vahdati, M. and Mirnia, M.J. 2023. Statistical analysis and optimization of variables affecting the end diameter of AISI 304 steel tube produced by flaring process. Amirkabir Journal of Mechanical Engineering. 54(12):2861-2876. doi:10.22060/MEJ.2022.21622.7479.

[39] Vahdati, M., Mahdavinejad, R. and Amini, S. 2015. Statistical analysis and optimization of factors affecting the spring-back phenomenon in UVaSPIF process using response surface methodology. International Journal of Advanced Design and Manufacturing Technology (ADMT). 8(1):13-23.

[40] D'Addona, D., Raykar, S.J., Singh, D. and Kramar, D. 2021. Multi Objective Optimization of Fused Deposition Modeling Process Parameters with Desirability Function. Procedia CIRP. 99(1):707-710. doi:10.1016/j.procir.2021.03.117.